Pressure induced $Fe^{2+}+Ti^{4+} \rightarrow Fe^{3+}+Ti^{3+}$ intervalence charge transfer and the Fe^{3+}/Fe^{2+} ratio in natural ilmenite ($FeTiO_3$) minerals

2004 J. Phys.: Condens. Matter 16 2707

(http://iopscience.iop.org/0953-8984/16/15/021)

INSTITUTE OF PHYSICS PUBLISHING JOURNAL OF PHYSICS: CONDENSED MATTER

J. Phys.: Condens. Matter **16** (2004) 2707–2718 PII: S0953-8984(04)75812-9

Pressure induced $Fe^{2+} + Ti^{4+} \rightarrow Fe^{3+} + Ti^{3+}$ intervalence charge transfer and the Fe^{3+}/Fe^{2+} ratio in natural ilmenite ($FeTiO_3$) minerals

Takele Seda[1,3] **and G R Hearne**[2]

[1] Western Washington University, Department of Physics and Astronomy, Bellingham, WA-98225, USA
[2] School of Physics, University of the Witwatersrand, Private Bag X3, Wits-2050 Johannesburg-Gauteng, South Africa

E-mail: sedat@physics.wwu.edu

Received 10 February 2004
Published 2 April 2004
Online at stacks.iop.org/JPhysCM/16/2707
DOI: 10.1088/0953-8984/16/15/021

Abstract

The Fe^{3+}/Fe^{2+} ratio in natural ilmenite ($FeTiO_3$) samples shows rapid increase under pressure from ambient up to ∼2 GPa, as deduced from ^{57}Fe Mössbauer pressure studies. The ratio, which is initially 0.2 at ambient pressure, saturates at ∼0.65 beyond 2–4 GPa to the highest pressure of 14 GPa in this study. Dramatic changes occur at low pressure where the compressibility of the unit cell is appreciably anisotropic, the *c*-axis being more compressible than the *a*-axis, and coincides with the rapid decrease observed in the electrical resistance under pressure. Pressure induced intervalence charge transfer away from the ferrous sites, conceivably across regions of octahedra, to the empty 3d manifold of the Ti^{4+} cation in an adjacent face-sharing layer along the *c*-axis may account for the change in the Fe^{3+}/Fe^{2+} ratio.

1. Introduction

Ilmenite is a common mineral in nature as an accessory phase in the most basic igneous and metamorphic rocks, therefore, has fundamental importance in the study of rock magnetism [1, 2]. It usually shows solid solutions towards Fe_2O_3, the proportion of which reflects the oxygen fugacity of the Earth's mantle. Both ilmenite and hematite have a NiAs structure derivative with a rhombohedral unit cell in that the oxygen ions are approximately hexagonally close-packed along the *c*-axis and the cations occupy two-third of the octahedral sites.

$FeTiO_3$ crystallizes in ilmenite, lithium-niobate and unquenchable perovskite structures depending on the pressure–temperature conditions with ilmenite as a stable phase at ambient

[3] Author to whom any correspondence should be addressed.

conditions and perovskite at high-pressure and room temperature [3]. Synchrotron x-ray diffraction measurements in a diamond anvil cell at room temperature [4] shows a reversible structural phase change from lithium-niobate to perovskite at 16 GPa with a volume change of -2.8% and the strongest x-ray peaks from the lithium-niobate phase persisting up to 20 GPa. Single crystal x-ray structural refinement [5] indicates that the mean Fe–O and Ti–O distances increase linearly with temperature and decrease linearly with pressure, the mean Fe–O being about twice as expandable and compressible as the mean Ti–O.

Synthetic ilmenite at ambient conditions gives a doublet Mössbauer spectrum with isomer shift of 1.04 mm s^{-1} with respect to α-Fe and quadrupole splitting of 0.88 mm s^{-1} [6]. With pressure, there is a decrease in the isomer shift attributed to an increase of the s-electron density at the nuclear site and the quadrupole splitting increases by 75% in the first 10 GPa. Low temperature Mössbauer measurement on doped material with magnesium [7] shows a sudden increase in quadrupole splitting below the Néel temperature and at 4.2 K the effective hyperfine field is found to be 5.6 T. A Mössbauer study on quenched samples of $(1-x)Fe_2O_3$–$xFeTiO_3$ from 1150 °C indicated that samples with the composition $x > 0.5$ are antiferromagnetic below the magnetic ordering temperatures [8]. This composition range exhibits electron transfer between Fe^{2+} and Fe^{3+} that continues up to $x = 0.6$. Samples in the range $0.25 \leqslant x \leqslant 0.5$ are ferrimagnetic at room temperature with the net magnetic moments aligned parallel to the (111) plane. No electron transfer was observed in the composition range $0.6 \leqslant x \leqslant 1$.

Determination of the ratio of the oxidation states of the two mineralogically important iron cations (Fe^{3+}/Fe^{2+}) has been one of the important methods in the study of iron bearing materials to get information about the weathering history of deposited minerals and the diagenesis of these materials after deposition at a particular location. This oxidation ratio could also be used as an indication of the pressure of formation when combined in high-pressure laboratory experiments like the DAC. Ilmenite, $FeTiO_3$, is one of the iron-bearing minerals with iron naturally occurring in the two oxidation states (Fe^{3+} and Fe^{2+}), hence it is good candidate for studying the Fe^{3+}/Fe^{2+} ratio *in situ* under pressure. It is a mineral commonly found as rock inclusion in kimberlites and volcanic rocks. The oxidation state of the ilmenite mineral inclusion is, therefore, indicative of the oxidation state of the host kimberlite assemblage, which in turn determines the origin and genesis of diamond.

In this study we examine the oxidation states of iron in ilmenite at high-pressure, closely representative of the mantle pressure conditions under which diamonds are formed. We study the pressure evolution of the oxidation states of iron and the Fe^{3+}/Fe^{2+} ratio in natural ilmenite mineral assemblages to a pressure of ~14 GPa (~400 km deep) using ^{57}Fe Mössbauer spectroscopy in a diamond anvil cell and elucidate the nature of electrical transport by measuring the electrical resistance at variable high-pressures as a function of temperature in a gem anvil cell.

2. Experimental details

A mineral assemblage of ilmenite from the Hillindale mining area of Kwazulu-Natal, South Africa has been used in this study. Some of the material has been heat treated at ~650 K to increase the ferric content. X-ray diffraction studies show minor contributions from rutile, TiO_2, and hematite, Fe_2O_3, as impurity phases [9]. The dominant phase is ilmenite having lattice parameters of $a = 5.085(34)$ Å and $c = 14.0567(23)$ Å for the unit cell of this compound. ^{57}Fe Mössbauer spectra have been recorded at ambient pressure on ~10 mg cm^{-2} of sample at room temperature. A theoretical fit to the spectrum exhibits two paramagnetic components and a much less abundant magnetically split component (see tables 1 and 2). One of the paramagnetic components with isomer shift $\delta = 1.06(1)$ mm s^{-1} and quadrupole

Table 1. Abundance of each component of the spectra of a heat-treated sample derived from the absorption areas at room temperature and variable pressure. The isomer shifts with respect to α-Fe and quadrupole splitting for the ferrous and ferric components, as well as the line-widths for the ferrous components, are also tabulated.

P	Abundances (%)			δ (mm s^{-1})		ΔE_Q (mm s^{-1})		Γ_A
(GPa)	Fe^{2+}	Fe^{3+}	Fe_2O_3	Fe^{2+}	Fe^{3+}	Fe^{2+}	Fe^{3+}	(Fe^{2+})
Ambient	74.2	16.1	9.7	1.067(1)	0.272(8)	0.694(2)	0.32(2)	0.345(4)
0.2	61.2	26.7	12.1	1.011(7)	0.13(2)	0.68(1)	0.33(3)	0.31(2)
1.5	55.8	30	14.2	1.00(1)	0.05(1)	0.79(1)	0.31(2)	0.37(2)
5.3	55.8	34.1	9.8	0.99(1)	0.02(1)	0.87(2)	0.26(3)	0.37(2)
8.6	53.1	34.4	12.5	0.985(8)	0.008(8)	0.95(1)	0.21(2)	0.41(2)
12	55.3	35.4	9.3	0.98(1)	−0.026(7)	1.08(2)	0.16(2)	0.51(2)
14	53.4	36.5	10.1	0.972(2)	−0.027(5)	1.14(1)	0.16(2)	0.56(2)

Table 2. Abundance of each component of the spectra of an untreated sample at room temperature and variable pressure. The isomer shifts with respect to α-Fe and quadrupole splitting for the ferrous and ferric components, as well as the line-widths for the ferrous components, are also tabulated.

P	Abundances (%)			δ (mm s^{-1})		ΔE_Q (mm s^{-1})		Γ_A
(GPa)	Fe^{2+}	Fe^{3+}	Fe_2O_3	Fe^{2+}	Fe^{3+}	Fe^{2+}	Fe^{3+}	(Fe^{2+})
Ambient	72.2	13.2	14.6	1.021(1)	0.21(1)	0.693(2)	0.39(2)	0.311(3)
1.1	65.9	19.1	15	0.987(6)	0.06(1)	0.80(2)	0.30(3)	0.29(1)
3.5	63.1	22.7	14.2	0.990(4)	0.11(1)	0.830(6)	0.33(2)	0.299(9)
6.0	59.8	26.7	13.5	0.985(4)	0.12(1)	0.884(7)	0.33(2)	0.32(1)
8.2	57	29.2	13.8	0.99(1)	0.077(9)	0.96(1)	0.31(2)	0.43(1)
9.4	58	28.7	13.3	0.99(4)	0.044(6)	1.033(6)	0.23(1)	0.42(1)
12	55.6	29.1	15.3	0.985(7)	0.006(5)	1.099(7)	0.17(1)	0.448(9)
14	56.1	30.4	13.5	0.977(4)	−0.018(4)	1.169(7)	0.14(2)	0.49(1)

splitting $\Delta E_Q = 0.69(1)$ mm s^{-1}, attributed as the ferrous iron and the other component with $\delta = 0.27(2)$ mm s^{-1} and $\Delta E_Q = 0.32(1)$ mm s^{-1} attributed as ferric iron. The isomer shifts have been quoted relative to α-Fe. These values are in close accord with those reported in the literature [6]. There was no change in the spectrum after measuring some of the sample that had been ground into a fine powder under acetone.

For ^{57}Fe Mössbauer measurements some of the fine powder was loaded into a 300 μm × 50 μm cavity drilled in a TaW gasket mounted for pressure studies in a miniature Merrill–Basset-type cell. Fine ruby powder was also loaded into the sample cavity to act as a pressure marker using the ruby luminescence line shift of the R_1 line. Liquid-argon was loaded into the sample cavity to ensure a quasi-hydrostatic pressure environment. The pressure distribution within the sample cavity was checked by measuring a number of ruby granules distributed throughout the cavity. The pressure distribution was typically 5–10% of the average pressure in the cavity. For the Mössbauer experiments at room temperature the miniature cell was accommodated at the end of a vertically oriented sample holder. This could also be inserted into a cryostat for variable cryogenic temperature ^{57}Fe Mössbauer pressure studies down to 4 K [10]. A customized point source ^{57}Co(Rh) of ∼10 mCi was used in conjunction with a Kr–CO_2 proportional counter for all the transmission Mössbauer experiments. ^{57}Fe Mössbauer spectra have been recorded at selected pressures up to 14 GPa at room temperature.

In the analysis of the spectra, the full transmission integral has been used, as part of the fitting program NORMOS (distributed by WissEl—Wissenschaftliche Elektronik GmbH,

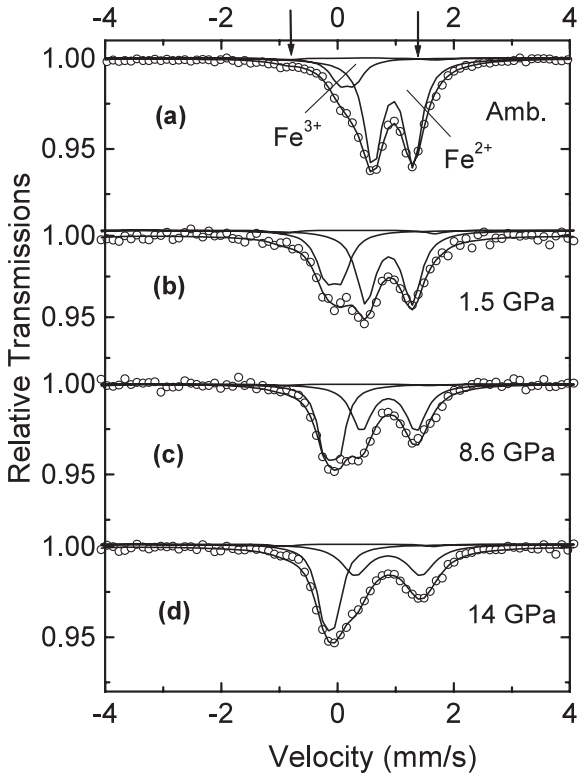

Figure 1. Pressure evolution of ^{57}Fe Mössbauer spectra of a heat-treated $FeTiO_3$ sample at room temperature plotted on a restricted velocity scale to more clearly show the ferrous and ferric components. Solid curves are theoretical fits to the experimental data. The ferrous and ferric components have been shown in the spectra at ambient conditions. The inner lines of the magnetic sextet component of Fe_2O_3 are barely discernible and their positions are only shown by arrows in the spectrum at ambient conditions. The spectra show a pronounced increase in the relative intensity of the ferric component with pressure.

Germany). This takes into account thickness effects and has been used to obtain the hyperfine interaction parameters and absorption areas. A source line width of 0.16 mm s^{-1} has been used in the theoretical fits to the data. In our resistance–pressure experiments four-probe current-reversing resistance–temperature (R–T) measurements have been performed with a dip-stick-type arrangement in a storage Dewar using cubic-zirconia gems as pressure anvils, fine gold-wire electrodes and insulating mica gaskets to constitute the confining sample cavity [11].

3. Results

3.1. High-pressure ^{57}Fe Mössbauer spectroscopy

^{57}Fe Mössbauer spectra recorded at selected pressures are plotted in figures 1 and 2 for the heat-treated and untreated samples, respectively. The spectra have been plotted on a small velocity scale to show the pressure evolution of the ferrous and ferric components very clearly. These two components are indicated in the spectra at ambient conditions. Due to the restricted velocity scale used the most intense outer lines of the magnetic sextet hematite—Fe_2O_3 component are

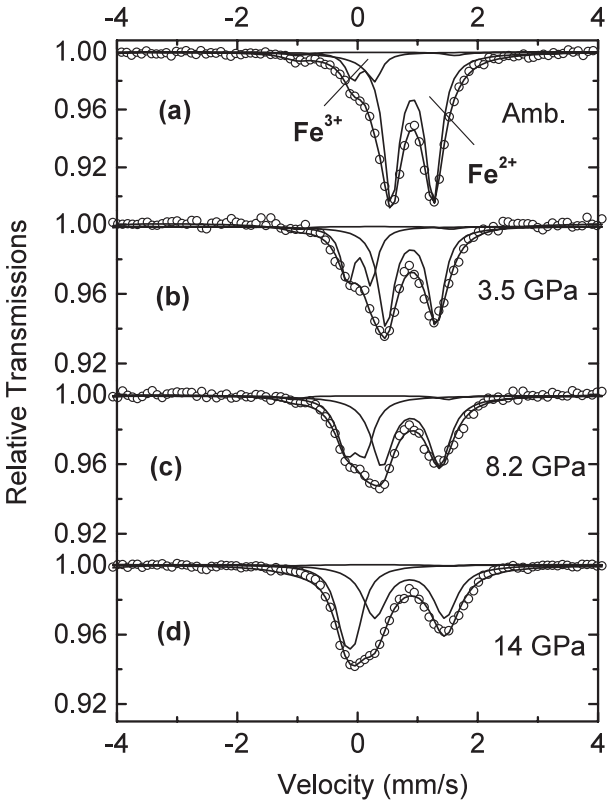

Figure 2. Pressure evolution of ^{57}Fe Mössbauer spectra of an untreated $FeTiO_3$ sample at room temperature plotted on a restricted velocity scale. The spectra show a pronounced increase in the relative intensity of the ferric component with pressure, similar to the behaviour observed in the heat-treated sample in figure 1. Solid curves are theoretical fits to the experimental data.

not visible and only the inner lines are barely discernible. These two inner lines are indicated in the spectrum at ambient conditions by arrows from the top in figure 1.

The hyperfine interaction parameters for the ferrous and ferric components as obtained from the analyses of the spectra are given in table 1 for the heat-treated sample and in table 2 for the untreated sample, respectively. The abundances of each of the three components along with the spectral line-width for the ferrous component are also included in the tables. It is clear from the figures that there is a pronounced increase in the intensity of the ferric component and a corresponding decrease in the intensity of the ferrous component with increasing pressure for both samples. The abundance of each of the three spectral components, as derived from the absorption areas in the theoretical fit to the data is plotted in figure 3 for the heat-treated sample.

Both the heat-treated and untreated samples show similar behaviour under pressure (compare figures 1 and 2; tables 1 and 2). Therefore, only the abundances and the hyperfine interaction parameters of the ferrous and ferric components for the heat-treated sample are shown in figures 3 and 4. It is obvious from figure 3(b) that the absorption area of the ferric component increases appreciably at lower pressures and there is a corresponding decrease in the absorption area of the ferrous component. The abundance approaches saturation above $\sim$4 GPa for both the ferric and ferrous components. This can be observed clearly in the change

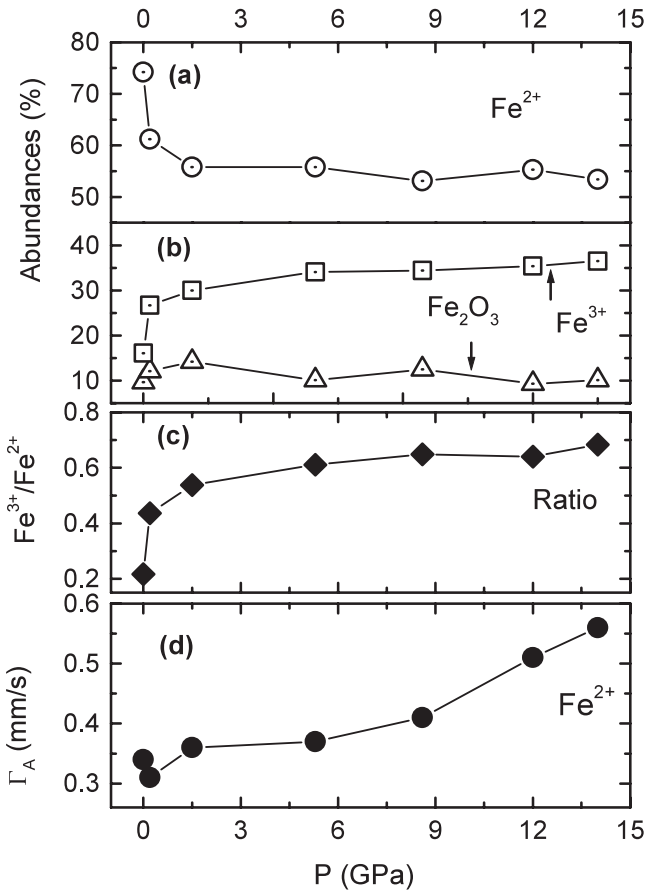

Figure 3. Pressure variation of the abundance of the ferrous and ferric components for the heat-treated sample as derived from the absorption areas of the components of each spectrum in figure 1. The ferric-to-ferrous ratio is also plotted in (c). The line-width Γ_A of the ferrous component shown in (d) is seen to exhibit appreciable broadening as pressure rises beyond ∼4 GPa. Solid curves through the data points are guides to the eye.

of the Fe^{3+}/Fe^{2+} ratio shown in figure 3(c). The ratio increases from ∼0.2 at ambient pressure to ∼0.65 at 14 GPa corresponding to the changes in the absorption areas. The abundance of the magnetic component (Fe_2O_3) remains almost constant throughout the pressure range studied here.

The possible explanation for the increase in the ferric abundance and the corresponding decrease in the ferrous abundance may be due to pressure-induced intervalence charge transfer between face-sharing octahedra of the Fe and Ti cations [12]. Equivalently, an alternative explanation is a pressure-induced chemical reaction of the form:

$$\tfrac{1}{2}O_2 + 2FeTiO_3 \rightarrow Fe_2O_3 + 2TiO_2$$

where the Fe_2O_3 end product of the reaction is meant to signify an increase in ferric content as part of a Fe_2O_3–$FeTiO_3$ solid solution series. Micro-Raman experiments have been performed on the sample at the highest pressure of this study and a Debye–Scherrer image on the untreated sample decompressed from 14 GPa to ambient conditions has been recorded and compared with the original sample at ambient pressure. There is no evidence of an increase in TiO_2

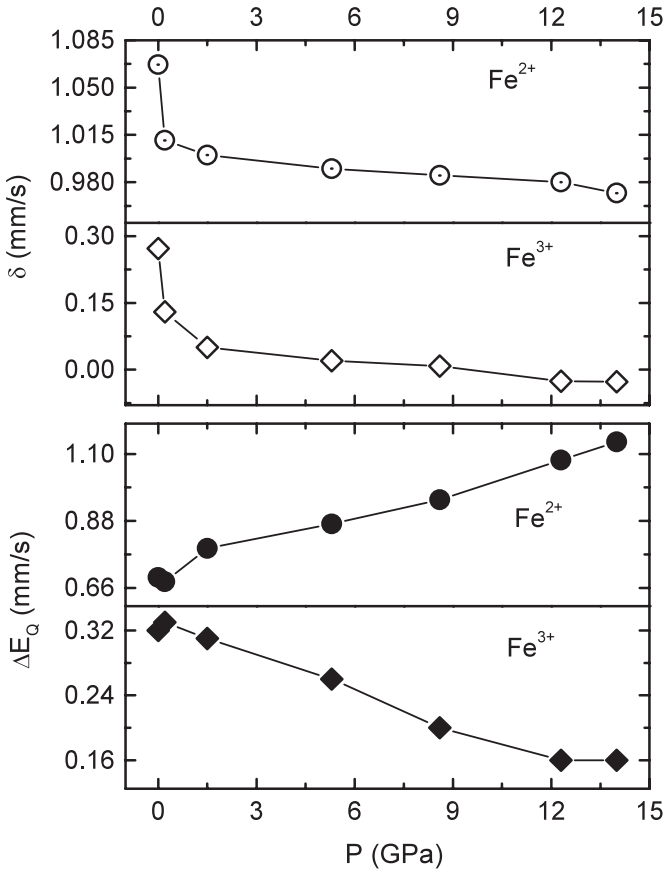

Figure 4. Pressure variation of the isomer shift (δ) with respect to α-Fe and quadrupole splitting (ΔE_Q) for both ferrous and ferric components of the heat-treated sample. The isomer shifts decrease with increasing pressure, indicating an increase in the electron density at the Fe nucleus while the quadrupole splitting increases with pressure for the ferrous component and decreases for the ferric component. Solid curves through the data points are guides to the eye.

content suggested by the above reaction to more than the dilute impurity content of less than 5% that exists in the original materials. Therefore, the possibility of the above oxidation reaction taking place under pressure in our $FeTiO_3$ samples seems unlikely.

The spectral line-width for the ferrous component is plotted in figure 3(d) as a function of pressure. The line-width shows appreciable broadening as pressure rises beyond 4–5 GPa. The broadening is independent of the line-width of the ferric component. The ferrous component shows similar broadening whether the line-width of the ferric component is permitted to vary in the fitting procedure or fixed at the ambient condition value. Neither the ferric component nor the magnetic sextet hematite component shows this broadening under pressure.

The isomer shift relative to α-Fe and quadrupole splitting for the ferrous and ferric components as extracted from the theoretical analyses of the spectra are plotted in figure 4 for the heat-treated sample. The isomer shift shows similar behaviour for both the ferrous and ferric components decreasing with increasing pressure indicative of increasing electron density at the nuclei of both components. The isomer shifts decrease appreciably below $\sim$2 GPa where abundances of the components also show pronounced changes. The change in the isomer

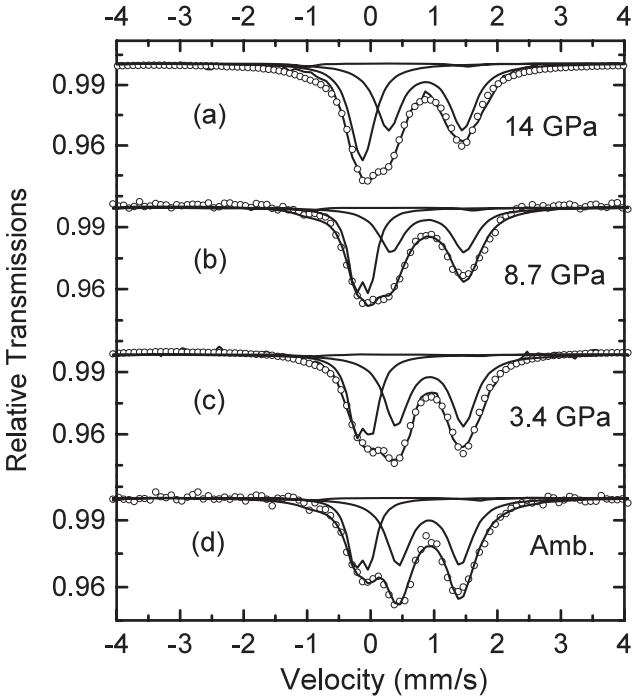

Figure 5. ^{57}Fe Mössbauer spectrum of untreated $FeTiO_3$ recorded on pressure release from 14 GPa (a) to ambient pressure (d). The spectrum shows relaxation, but does not fully recover to its ambient condition form in figure 2(a).

shifts is monotonic above 2 GPa for both samples. The electric quadrupole splitting for the ferrous component increases with pressure, whereas for the ferric component it decreases with increasing pressure. The difference in the behaviour of the quadrupole splitting under pressure for the two components may be referred to their difference in the valence contribution to the electric field gradient [13].

Figure 5 is ^{57}Fe Mössbauer spectra of the untreated sample recorded at room temperature on pressure release from 14 GPa. It is evident from the evolution of the spectra that the areas under the curve for both the ferrous and ferric components show slight but significant changes as the pressure is released progressively. The abundances of each component obtained from the analysis of the spectrum decompressed to ambient pressure in figure 5(d) are 66.3% Fe^{2+}, 19.7% Fe^{3+} and 14.0% Fe_2O_3. Comparison of these values to the corresponding values of 72.2%, 13.2% and 14.6%, respectively, at ambient conditions before application of pressure (see table 2), shows that there is still a significant increase in the ferric component and a corresponding decrease in the ferrous component after the pressure is fully released to ambient conditions. On the other hand, when compared to the values of 56%, 31% and 13% respectively at 14 GPa in figure 5(a) and table 2, there is a significant increase in the abundance of the ferrous component and a corresponding decrease in the ferric component of the decompressed spectrum. This implies that there is some relaxation in the spectra on decompression due to the relief of the stress, but the spectrum does not fully recover to its ambient condition form. Spectra recorded on the decompressed sample several months after decompression shows the same values for the hyperfine interaction parameters as the spectrum in figure 5(d). The irreversible nature of the transition is probably due to a residual strain.

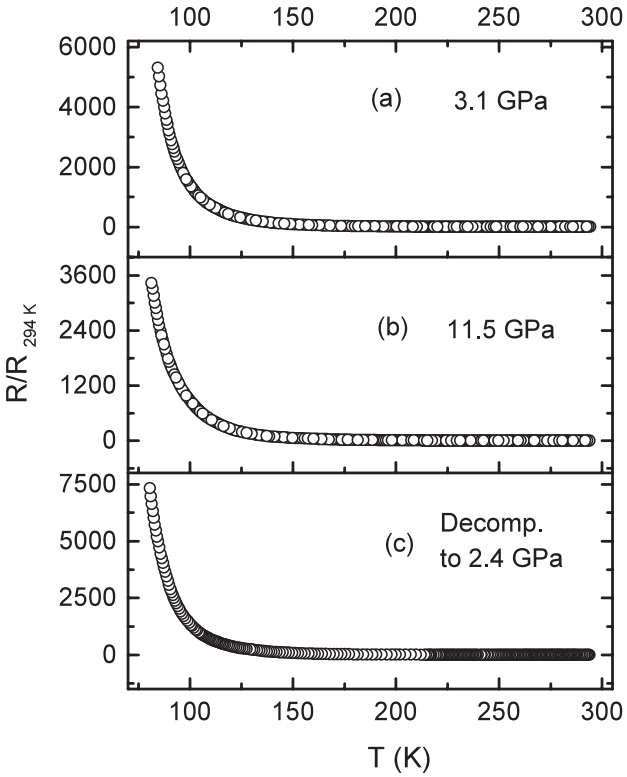

Figure 6. Normalized electrical resistance data of the untreated $FeTiO_3$ at selected pressures as a function of temperature: (a) and (b) upon increasing pressure at 3.1 and 11.5 GPa respectively. In both cases the data show that the resistance increases with decreasing temperature, typical behaviour of a non-metallic material. The data in (c) is recorded after pressure release to 2.4 GPa, indicating the reversible behaviour of the resistance on decompression.

3.2. High-pressure electrical resistance

Resistance data normalized to the value at 294 K are plotted in figure 6 as a function of temperature. The data in figures 6(a) and (b) are the resistance values at 3.1 and 11.5 GPa, respectively, of the untreated sample after grinding into a fine polycrystalline powder. The resistance increases with decreasing temperature, thus obtaining a negative temperature coefficient for the whole pressure measured. The increase in the resistance is high at low temperatures and it is ∼3.5 orders of magnitude near 80 K as compared to the value at room temperature, typical of semi-conducting materials with small band gap. The data in figure 6(c) is recorded after pressure release from 11.5 to 2.4 GPa. It is clear from the figure that the normalized resistance value is higher on decompression when compared to the value at 11.5 GPa, indicating the reversible behaviour of the resistance to its low-pressure values when the stress is released; an intrinsic property of the material.

Due to a decrease in atomic distances and an increase of atomic orbital overlap under pressure, the resistance of materials is expected to decrease. Previous resistance–pressure studies [14] on synthetic samples of ilmenite show that there is an appreciable decrease in resistance of ∼2.5 orders of magnitude as a function of pressure to ∼5 GPa. Our result shows a similar trend, where there is significant decrease in resistance with increasing pressure at

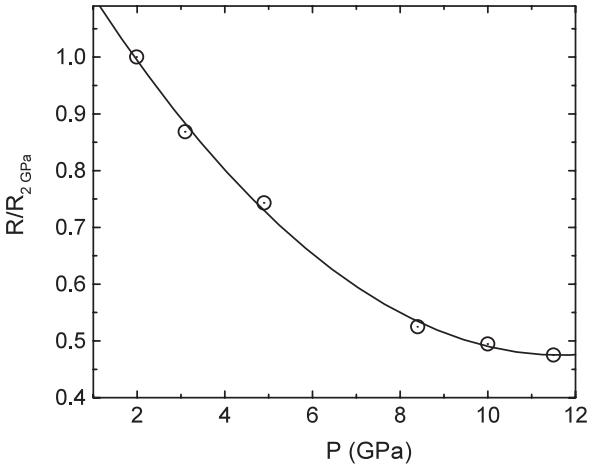

Figure 7. Room temperature electrical resistance of untreated $FeTiO_3$ as a function of pressure normalized to the resistance value at 2 GPa, indicating a decrease in the resistance with increasing pressure. Open circles are data points and the solid curve is a non-linear fit to the data.

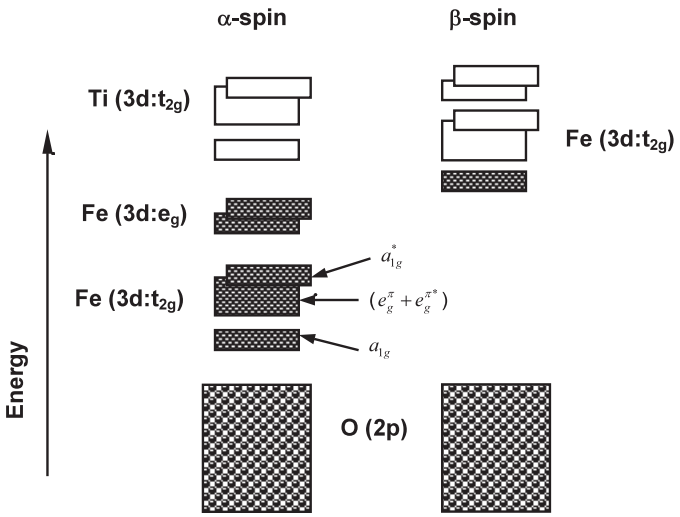

Figure 8. Energy band scheme of the cation 3d sub-bands of ilmenite, $FeTiO_3$, at ambient pressure. Occupied states are shown shaded and unoccupied states are left unshaded.

room temperature, as shown in figure 7. The resistance value at 3.1 GPa is ∼2.3 times the value at 11.5 GPa at room temperature.

4. Discussion and conclusions

Structural refinements up to 1050 °C at ambient pressure and up to ∼4.6 GPa at room temperature in separate experiments have shown that the unit-cell compression in $FeTiO_3$ is quite anisotropic, being more compressible along the c-axis compared to the a-axis perpendicular to this [5]. The anisotropy in unit-cell compression is reflected in a decrease of the c/a ratio with rising pressure, primarily because of the reduced rigidity between upper and

lower oxygen layers along the c-axis of the FeO_6 local environment compared to that of the TiO_6 octahedron which tends to constrain deformation in the a-axis direction. The anisotropic compression when pressure is applied to the unit cell is expected to be associated with more substantial shortening of metal–metal distances along c-axis (i.e. Fe–Ti across shared-faces) than between adjacent metal sites (Fe–Fe or Ti–Ti) across shared edges. There is $\sim$1.04% reduction in the face-shared Fe–Ti distances as compared to the $\sim$0.57% and $\sim$0.65% reduction in the edge-shared Fe–Fe and Ti–Ti distances, respectively, from ambient to $\sim$4.6 GPa.

The magnetic and electrical transport of $FeTiO_3$ is expected to depend on the possible variation of Fe^{3+} due to the solid solution between $FeTiO_3$ and Fe_2O_3 where Fe^{3+} substitutes both Fe^{2+} and Ti^{4+} in their respective sites. Even in the non-stoichiometric end member $FeTiO_3$, due to the presence of different alternating cation sites (Ti^{4+} and Fe^{2+}) and the additional existence of a finite Fe^{3+} cation, excitation of electrons by visible light [15] or application of external pressure is expected to facilitate the metal–metal intervalence charge transfer between these cations as a result of the increase in overlap of atomic orbitals [16, 17].

The increase in the ferric component and corresponding decrease in the ferrous component in $FeTiO_3$ as a function of pressure may, therefore, be ascribed to an intervalence charge-transfer mechanism of the type $Fe^{2+} + Ti^{4+} \rightarrow Fe^{3+} + Ti^{3+}$ [18]. This type of intervalence charge-transfer at ambient pressure has been considered in molecular orbital calculations by Sherman [12] for $FeTiO_3$ and experimentally observed in other minerals containing both Fe^{2+} and Ti^{4+} cations [19]. It has been shown to involve a $Fe^{2+} \rightarrow Ti^{4+}$ charge-transfer energy of $\sim$18 000 cm^{-1} (i.e. $\sim$2.2 eV), and compares favourably with the optical absorption energies that occur in visible-region (15 000–21 000 cm^{-1}) spectra at room temperature of numerous minerals incorporating Fe and Ti, when light is polarized along metal–metal directions in the crystal structure. The Fe^{3+}/Fe^{2+} ratio in our Mössbauer spectra tends to saturate above $\sim$4 GPa from $\sim$0.2 at ambient to $\sim$0.65 at 14 GPa corresponding to a change of $\sim$0.45. This value agrees well with the valence delocalization coefficient, α, of 0.5 estimated by Sherman [12] for complete delocalization of the Fe^{2+} β-spin electrons onto the Ti atom.

A Mössbauer study of the $(1 - x)Fe_2O_3$–$xFeTiO_3$ series [8] showed that all Fe^{2+} ions in Fe_2O_3-rich samples participate in electron transfer with an equal number of Fe^{3+} ions. This electron transfer continues for the value of x as great as 60%, but no electron transfer between Fe^{2+} and Fe^{3+} cations is observed in the compositional range $0.75 < x < 1.0$. In the range $0 < x < 0.6$, the cations are believed to be completely disordered so that $Fe^{2+} \rightarrow Fe^{3+}$ electron transfer occurs between both the face-shared and edge-shared octahedra. Cation ordering increases in the range $0.6 < x < 0.75$, with the result that $Fe^{2+} \rightarrow Fe^{3+}$ electron transfer between face-shared octahedra predominates. In the range $0.75 < x < 1.00$, Ti efficiently blocks electron transfer between $Fe^{2+} \rightarrow Fe^{3+}$ ions. The mechanism of electron transfer in this later range was not clear until a prominent broad band around 16 000 cm^{-1} of ilmenite was attributed to a $Fe^{2+} \rightarrow Ti^{4+}$ intervalence transition [18].

Within the ligand field picture, the nearly octahedral co-ordination of O atoms around the cations splits their 3d levels into a lower t_{2g} and upper e_g manifold separated from each other by the '$10Dq$' crystal-field splitting parameter [20]. For a given orbital, the spin-up (α) and spin-down (β) electrons will have an energy difference corresponding to the intra-atomic exchange energy. Predominant compression along the c-axis in the ilmenite structure [5], which corresponds to a trigonal distortion of the MO_6 octahedra, further splits the t_{2g} sub-bands into non-degenerate a_{1g} (bonding—a_{1g} and antibonding—a_{1g}^*), and a doubly degenerate π-bonding e_g (e_g^{π} and $e_g^{\pi *}$) sub-bands as shown in figure 8 [21]. The a_{1g} orbitals form (ddσ)-type bonds between the Fe and Ti cations of face-sharing octahedra that occur along the c-axis.

These a_{1g} orbitals directed nearly along the c-axis will experience more overlap as a function of pressure than those orbitals projected perpendicular to the c-axis, i.e. those orbitals

directed toward the common edge of neighbouring FeO_6 or TiO_6 octahedra. The Ti^{4+} cation has an unoccupied 3d shell, and the screened Coulomb attraction of the Fe^{2+} β-spin electron by a Ti^{4+} cation will be greater than, for example, the case of a Fe^{3+} cation for a given metal–metal distance. Therefore, the possibility of electron transfer in ilmenite of the Fe^{2+} β-spin electron to an unoccupied Ti^{4+} α-spin orbital may be enhanced under pressure as a result of increased a_{1g} orbital overlap, which may result in the decrease of the ferrous Fe and an increase in that of the ferric Fe.

Finally, we recommend further studies involving electronic structure calculations using, e.g., the potential energy surface given in Sherman [12] at high-pressure to have a full understanding of the electronic transition in ilmenite under pressure, whether it is due to purely static band overlap or vibronic processes. The irreversible nature of the electronic transition observed in the Mössbauer spectra also needs further investigation. Combined high-pressure and high-temperature ^{57}Fe Mössbauer study is necessary to investigate if the sample can fully relax when heated in vacuum or under inert atmosphere. It is also important to investigate similar materials of different origin at high-pressure to know if such an intervalence charge transfer process is universal in natural ilmenite samples or typical only to the current material.

References

[1] Lawson C A 1981 *Science* **213** 1372
[2] Burton B 1984 *Phys. Chem. Minerals* **11** 132
[3] Metha A, Leinenweber K, Navrotsky A and Akaogi M 1994 *Phys. Chem. Minerals* **17** 207
[4] Leinenweber K, Utsumi W, Tsuchida Y, Yagi T and Kurita K 1991 *Phys. Chem. Minerals* **18** 244
[5] Wechster B A and Prewitt C T 1984 *Am. Mineral.* **69** 176
[6] Vaughan R W and Drickamer H G 1967 *J. Chem. Phys.* **47** 1530
[7] Syono Y, Ito A and Morimoro S 1981 *J. Phys. Chem. Solids* **42** 483
[8] Warner B N, Shive P N, Allen J L and Terry L 1972 *J. Geomagn. Geoelectr.* **24** 353
[9] Nell J and den Hoed P 1997 *Heavy Minerals* ed R E Robinson (Johannesburg: The South African Institute of Mining and Metallurgy)
[10] Hearne G R, Pasternak M P and Taylor R D 1994 *Rev. Sci. Instrum.* **65** 3787
[11] Reichlin R L 1983 *Rev. Sci. Instrum.* **54** 1674
[12] Sherman D M 1987 *Phys. Chem. Minerals* **14** 364
[13] Ingalls G 1964 *Phys. Rev.* **133** A787
[14] Boekema C, Woude F v d and Sawatzky G A 1976 *J. Physique Coll.* **37** (Suppl. 12) C6
[15] Allen G C and Hush N S 1967 *Prog. Inorg. Chem.* **8** 357
[16] Smith G and Strens R G J 1976 *The Physics and Chemistry of Minerals and Rocks* ed R G J Strens (London: Wiley)
[17] Mao H K 1976 *The Physics and Chemistry of Minerals and Rocks* ed R G J Strens (London: Wiley)
[18] Burns R G 1981 *Annu. Rev. Earth Planet. Sci.* **9** 345
[19] Smith G 1977 *Can. Mineral.* **15** 500
[20] Burns R G 1993 *Mineralogical Applications of Crystalfield Theory* (Cambridge: Cambridge University Press)
[21] Mattheiss L F 1996 *J. Phys.: Condens. Matter* **8** 5987